Journal of Materials Chemistry A

Accepted Manuscript

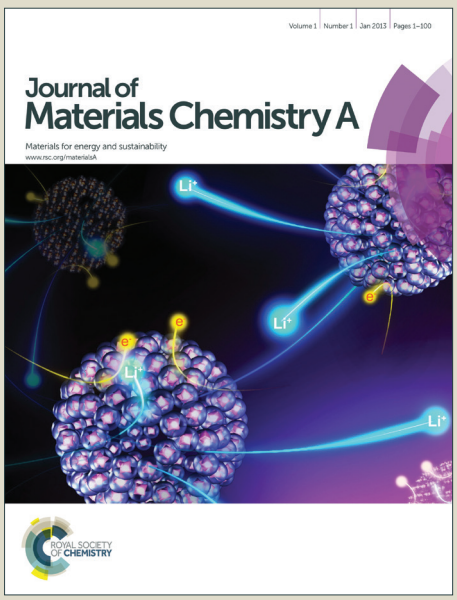

ROYAL SOCIETY OF CHEMISTRY

www.rsc.org/materialsA

Journal Name

ARTICLE

Aerosol assisted chemical vapour deposition of transparent conductive ZnO thin films with hexagonal microplate surface and ultrahigh haze value

Received 00th January 20xx,
Accepted 00th January 20xx

DOI: 10.1039/x0xx00000x

www.rsc.org/

Shuqun Chen,[a] Martyn McLachlan,[b] Andrei Sapelkin[c] and Russell Binions[a]*

We report a novel and facile aerosol assisted chemical vapour deposition (AACVD) approach to fabricate transparent, conductive ZnO thin films with highly hexagonal-plate-textured surfaces on silica glass substrates by using zinc-acetate-dihydrate, acetic-acid, denoized water and methanol as precursor solution.

Introduction

Transparent conducting oxides (TCO) are a unique class of materials based on metal oxides that exhibit both optical transparency and electrical conductivity.[1] One important application for transparent conductive oxides is function as front electrode in thin-film solar cells.[2] This is especially true when the TCO layer is surface textured because a rough surface can bring efficient light scattering inside the solar cell and, therefore, enhances light absorption along the longer scattering path, leading to an increase of the photo-generated current.[3,4] In order to obtain textured TCO thin films, two approaches, including the employment of controlled micro-/nano-structures and pre-/post- deposition chemical etching, are mainly investigated.[5,6] The latter is actually less favourable to be used since the additional process would increase the manufacturing cost considerably, and thus the deposition of naturally-textured TCO coatings has attracted greater attention. A proven example is the growth of transparent conductive B-doped ZnO films with random pyramidal texture by means of low pressure chemical vapour deposition (LPCVD), which has already been successfully employed in commercial silicon solar modules.[4,7,8] Unfortunately, the volatile zinc precursor diethylzinc (DEZ) they used is highly pyrophoric and expensive.[9,10] Therefore, continuous efforts are being made by the CVD community to explore novel cost-effective techniques and precursors for textured ZnO materials.

In this paper, we report for the first time that transparent conductive ZnO thin films with ultrahigh haze value can be systemised on silica glass substrates by using a facile aerosol assisted chemical vapour deposition method utilising inexpensive precursors *i.e.* zinc-acetate-dihydrate, acetic acid, deionized water in methanol. AACVD, a solution based variant of conventional CVD process, involves the generation of a liquid-gas aerosol containing small droplets of precursor mixture which is transported to a reactor chamber by carrier gas to undergo further reaction and film formation.[11–14] The advantages of employing AACVD technique to fabricate ZnO nanomaterials include the usage of low cost non-volatile precursors and the ease of controlling film growth.[15–18] For example, C.S. McNally et al. firstly reported that ZnO films with uniform regular hexagonal platelets (200-400 nm in diameter) could be synthesised on glass substrates by AACVD reaction of zinc-acetate, methanol and a common chemical surfactant cetyltrimethylammonium bromide (CTAB).[16] After that we fabricated highly pyramidal-textured AACVD ZnO coatings (haze factor 91.6%) on fluorine tin oxide (FTO) glass substrates by simply adding acetic acid (~6.7 vol.%) in zinc-acetate-dihydrate and methanol solution.[17] The use of different solvent also exhibited significant influence on the AACVD ZnO film growth, where low-viscosity solutions, i.e. ethanol, tended to promote grain agglomeration and high-viscosity solutions, i.e. isopropanol, helped form uniformly distributed grains.[19]

Based on the above observations, in current AACVD work, we surprisingly found that the addition of small amounts of acetic acid (~1.7 vol.%) and moderate amounts of deionized water (~6.7 vol.%) together in zinc solutions also produced highly surface-textured ZnO films, with a haze factor as high as 98.5%. Combining favourable optical transparency (~70% across visible region) and electrical conductivity (minimum sheet resistance ~60 Ω sq^{-1}), we believe that these hazy ZnO coatings have good potential to be employed as front electrode in thin films solar cells. It is worth mentioning that the textured AACVD ZnO film surfaces are composed by large well-defined hexagonal plates (~1 μm in diameter). This could make them highly desirable for gas sensor materials as well because 1) the hexagonal plates has been reported to display superior gas sensing performance over other crystal planes in ZnO,[20,21] and 2) AACVD technique has been widely used to deposit TCO materials on sensor substrates.[11,22]

[a] *School of Engineering and Materials Science, Queen Mary, University of London, Mile End Road, London, E1 4NS, UK. E-mail: r.binions@qmul.ac.uk.*
[b] *Department of Materials, Royal School of Mines, Imperial College London, London, UK.*
[c] *Department of Physics and Astronomy, Queen Mary University of London, London E1 4NS, UK.*

† Electronic Supplementary Information (ESI) available: See DOI: 10.1039/x0xx00000x

Table 1 Experimental, structural and optical parameters for the studied ZnO films.

Sample I.D.	Acetic acid (mL)	D.I. water (mL)	$R_{(RMS)}$ (nm)	T_{total} (%)	$T_{diffuse}$ (%)	Haze (%)
ZnO	0	0	11.9	72.4	3.2	4.4
ZnO-a	1	0	125.6	72.2	44.0	60.9
ZnO-aw	1	4	216.6	68.1	67.1	98.5

Experimental

Zinc-acetate-dihydrate (≫98%), acetic acid (≫99%) and methanol (anhydrous, 99.8%) purchased from Sigma-Aldrich were used as received. Deionized water was taken from Vivendi water purification system. Aqueous solutions for the AACVD experiments were prepared by dissolving 0.6 g zinc-acetate-dihydrate in 60 mL methanol with different amount of acetic acid and DI water (listed in Table 1). Precursor mist was created using an ultrasonic humidifier and transferred to the reaction chamber with flowing nitrogen gas (1.0 L min^{-1}). It is worth mentioning that the addition of D.I. water makes the precursor solution harder to aerosolize and hence prolongs the deposition time from 60±5 mins to 100±5 mins. Deposition was carried out on silica glass substrates (90 mm × 45 mm × 4 mm) at an optimized temperature of 450 °C.

Film crystal structure was investigated by X-ray diffraction (XRD) with patterns collected over 10-70° under CuKα radiation (λ= 1.542 Å). Film surface morphology and roughness were examined by scanning electron microscope (SEM) and atomic force microscope (AFM), respectively. UV/Vis direct and total transmittance (T_{direct} and T_{total}) spectra of films were recorded on a UV-Vis-NIR spectrometer (measuring wavelength range = 380-780 nm) with an integrating sphere. Film diffuse transmittance ($T_{diffuse}$) was then determined by subtracting the direct transmittance from total transmittance ($T_{diffuse} = T_{total} - T_{direct}$). The haze factor is defined as the ratio of diffuse transmittance to total optical transmittance (Haze = $T_{diffuse}$ / T_{total}). The average film visible light transmission (380-780 nm) was computed according to the British Standard EN 673. Photoluminescence (PL) spectroscopy was performed at room temperature using a micro-Raman system in co-ordination with a CW 325 nm He:Cd laser. Film sheet resistance was measured using a four-point probe technique.

Results and discussion

Fig. 1 presents the optical images of three studied ZnO films on glass surfaces. As observed, pure ZnO displays an uniform transparent area in the middle of substrate and this region becomes slightly opaque after adding acetic acid in precursor solution. Further addition of D.I. water produces ultra-hazy coating mainly at the first part of glass surface, indicating a change of film growth mechanism. We infer the introduction of high volume deionised water would increase the aerosol density considerably since the density of water (1.0 g cm^{-3}) is higher than that of methanol (0.79 g cm^{-3}),[23] whereby the precursor droplets was likely to be absorbed on the substrate immediately after entering into the reactor under the given flow rate. By comparison, the lighter precursor mist in another two depositions may obtain sufficient momentum to migrate to thermodynamically preferred region, normally the central area in the flowing chamber,[24] and yielding denser coatings.

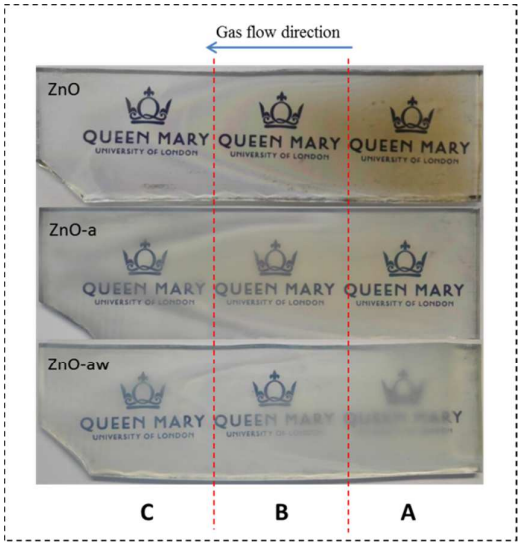

Figure 1 Optical appearance of studied ZnO films on glass substrates. The central area B in ZnO and ZnO-a as well as the beginning area A in ZnO-aw were selected for materials characterization.

To better characterize the initial optical observations, the UV-Vis total and diffuse transmittance of the ZnO films were measured and are illustrated in Fig. 2(a). The corresponding values are listed in Table 1. It is seen that all three samples exhibit similar high total transmission (68.1-72.4%) across visible region. By contrast, their diffuse transmission displays significant variations from an average value of 3.2% in pure ZnO to 44.0% in ZnO-a and 67.1% in ZnO-aw. In this regard, distinct haze spectra are presented in Fig. 2(b) and the haze factor for ZnO-aw was found to be as high as 98.5%, which is, to our best knowledge, the most hazy zinc oxide film so far reported.

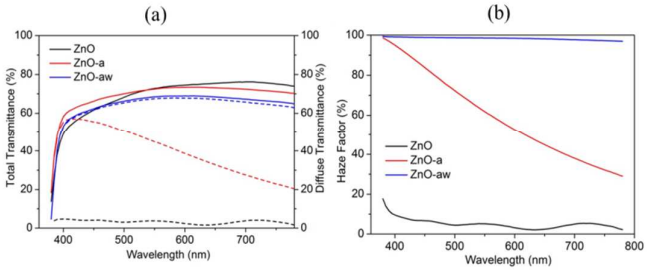

Figure 2 (a) UV-Vis total and diffuse transmittance and (b) haze factor spectra of studied ZnO films.

The structural properties of studied ZnO coatings, including surface and cross-section morphology as well as crystal orientations, were examined by SEM, AFM and XRD. As seen in Fig. 3(a), pure ZnO is largely composed by spherical agglomerated particles (~200 nm in diameter) and these agglomerates are formed

of refined rods around 100 nm in length, which are only visible under the high magnification. These wedge-like grains are quite different with previously reported disc-like ZnO crystals under similar AACVD conditions.[25] The corresponding XRD pattern in Fig. 3(d) exhibits a preferred growth direction along the $(10\bar{1}0)$ crystallographic plane, which may relate to its rod-like crystal growth.[26] The introduction of acetic acid results in uniform large tilted hexagonal plates (~1 μm in diameter) on ZnO-a film surface (see Fig. 3(b) and Fig. S1(a)). These hexagonal-plates are highly likely to be the base planes for ZnO pyramids because the side facets of hexagonal pyramid are clearly observed in the inset higher magnification image and the corresponding cross-section figure in Fig. S1(b). The evidence of pyramidal ZnO can be further verified from its diffraction pattern in Fig. 3(e), whose $(10\bar{1}1)$ peak intensity exceeds that of $(10\bar{1}0)$ and (0002), in accordance with previous report of ZnO pyramids.[27] The presence of deionized water in precursor solutions shows limited influence on the ZnO crystal size but helps fully expose the hexagonal plates. As shown in Fig. 3(c) and Fig. S1(c), the microscale plates are uniformly well-stacked along the normal direction, however the side-view for ZnO-aw (see Fig. S1(d)) illustrates the sample is thickened by large continuous grains. This indicates those overlapped plates only exist on the film surface instead of through the whole bulk area, which may explain why the XRD pattern of ZnO-aw in Fig. 3(f) exhibits an extremely strong peak along the [0001] direction instead of the $[10\bar{1}1]$.

From the AFM images in Fig. 3(g)-(i), the root mean square roughness (R_{RMS}) of ZnO, ZnO-a and ZnO-aw films are estimated to be 11.9 nm, 125.6 nm and 216.6 nm, respectively. Therefore, we can infer that the strong light trapping effect in ZnO-aw should result from its ultra-rough surface. It is noteworthy that, although ZnO-a has a similar roughness value to our previously reported pyramidal ZnO sample (RRMS ≈102 nm), the latter however exhibits a superior haze performance (91.5%) over ZnO-a (60.9%).[17] This indicates that surface roughness is not the only dominant parameter in determining film haze. The topography of light scatter also plays an essential role and in some cases maybe more dominant in determining film haze.

The nonpolar $\{10\bar{1}0\}$, semipolar $\{10\bar{1}1\}$ and polar $\{0001\}$ are the three main morphology-related surfaces in wurtzite ZnO. It is known that the polar facets intrinsically hold higher surface energy, thus zinc oxide usually tends to grow along the <001> or *c*-axis to minimize the $\{0001\}$ surface.[17] However, this preferential growth behaviour can be effectively modified with the assistance of organic species, leading to a variety of interesting ZnO nanostructures. The typical example is the promotion of *a*-axis oriented crystal growth by adding citrate ions in zinc precursor solutions, which have been proved to selectively adsorb on the {0001} facets and hinder crystal growth along the normal direction *c*-axis.[28–30] In other words, the citrates could lower the surface energy of polar {0001} facets by strong electrostatic interactions and make the hexagonal plates energetically favourable to be exposed. Besides the surface energy, a limited number of nucleation sites or slow nucleation behaviour at the first stage of deposition is also essential to obtain specific crystal morphology. This is not hard to understand because the reduced nucleation allows for more space to grow to large sizes in all orientations, and fast nucleation often results into refined particles, as illustrated in our untreated ZnO sample.

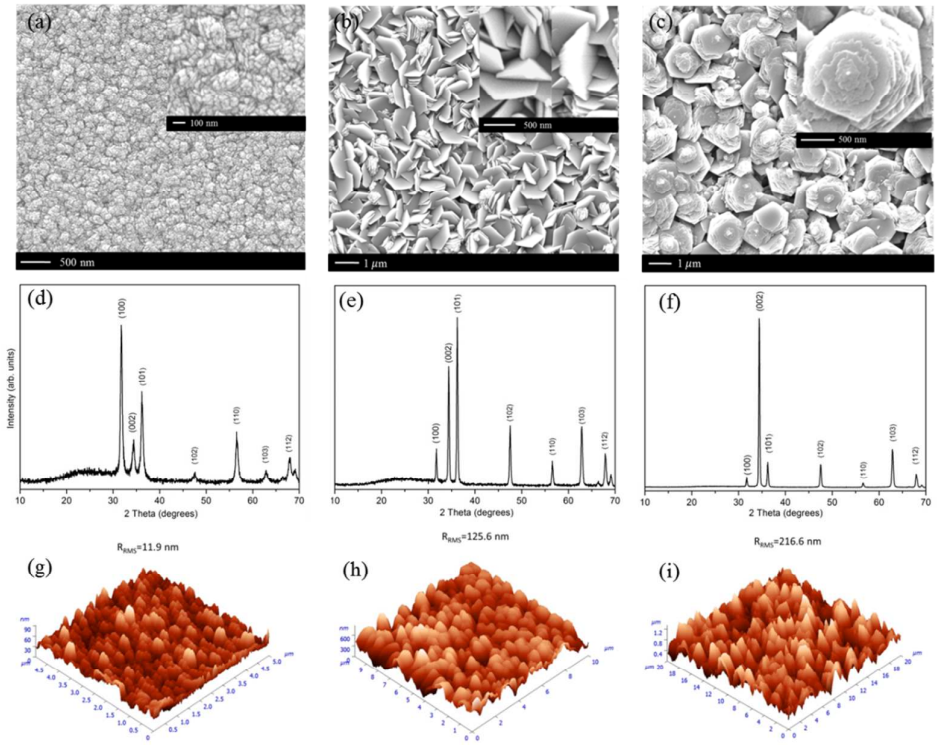

Figure 3 SEM, XRD and AFM images of (a), (d), (g) ZnO, (b), (e), (h) ZnO-a and (c), (f), (i) ZnO-aw films. All reflection signals match to ZnO with hexagonal wurzite structure (JCPDS 36-1451).

Similar to the citrates, the influence of acetates on the zinc oxide film growth and morphology is also profound and this has been demonstrated in our previous aacvd work[17] as well as among other relevant literature.[30,31] Thus, we could infer that the formation of hexagonal pyramids in ZnO-a should result from a retarded crystal nucleation and reduced polar surface energy with the assistance of capping acetate ions. The interactions between acetates and $\{0001\}$ facets may be more significant than that of $\{10\bar{1}1\}$ under given conditions, so the hexagonal base plates are more favourable to be exposed on the film surface instead of the pyramid side planes. The addition of D.I. water increases the aerosol density and narrows the film growth region at the beginning of glass surface. In this regard, a majority of acetate ions added may have reached the glass surface, since less acetic acid would be pre-decomposed because of the much shorter traveling distance within the reactor. This increase of acetate concentration would favour the *a*-axis oriented crystal growth, as suggested in the case of citrates,[28,30] and well-defined hexagonal plates are readily obtained. But during the film thickening process, these multistacked plates would simultaneously emerge into continuous *c*-axis oriented grains because the large interfacial area between polar $\{0001\}$ facets is energetically unstable. As a result, the reflection signals of $\{0001\}$ planes overwhelm that of $\{10\bar{1}1\}$ in the XRD pattern.

Finally, film electrical conductivity was evaluated by using the four-point probe method. Pure ZnO is relatively electrical resistant with resistance value exceeds MΩ sq^{-1} and the addition of acetic acid could effectively reduce it to ~2.3-4.1 KΩ sq^{-1}. The presence of D.I. water helps lower the film resistance tremendously to a minimum value of ~60 Ω sq^{-1}. This number is still a little high compared to those in previously reported ZnO:B front electrodes (~10-30 Ω sq^{-1}),[4,32] but considering that the reported samples (~ 2-4 μm) are much thicker than ours (~ 1 μm), a more conductive ZnO-aw sample can be anticipated once we prolong the deposition time. It is also worth mentioning that the ZnO-aw film resistance would increase linearly along the gas flowing direction, as illustrated in Fig. S2. This further supports our idea that the presence of deionized water could enhance the aerosol density considerably and thus the deposition area closer to the gas inlet receives more nucleuses. But for real industrial production, uniform deposits can be guaranteed by employing a more advanced aerosol delivery system.[33]

To explain the large variations in film conductivity, we examined the PL spectra of studied ZnO samples. As seen in Fig. 4, the ZnO-aw displays a board and intense peak near 520 nm, which has been reported to arise from a radiative recombination involving some lattice structural defects, such as oxygen vacancies, zinc vacancies, zinc interstitials.[34–36] This green emission peak becomes much less profound in ZnO-a and for the untreated ZnO sample the signals basically disappear into the background levels. According to previous studies, the zinc oxide samples with a large fraction of polar planes contain more oxygen vacancies.[21,37] A qualitative explanation to this phenomenon is that the ZnO polar planes stabilized by OH groups are subject to forming oxygen vacancies by removing either OH or H_2O groups from the surface.[37,38] Thus, combined our structural, electrical and photoluminescence results together, we could conclude that the low resistance in ZnO-aw should due to its high oxygen vacancy concentration with the formation of large polar hexagonal plates.

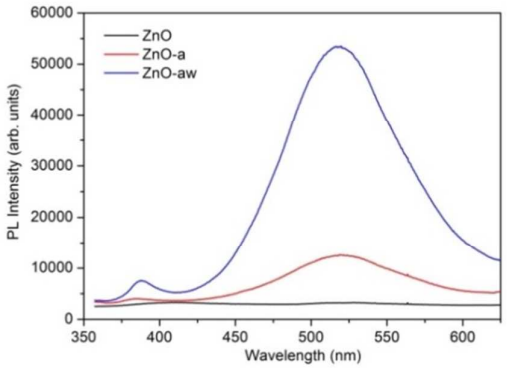

Figure 4 Room-temperature PL spectra of ZnO, ZnO-a and ZnO-aw films.

Conclusion

In summary, ZnO thin films with hexagonal-plate-shaped rough surfaces were successfully deposited on silica glass substrate by AACVD process. The coatings exhibit high visible transparency (~70%), low sheet resistance (~60 Ω sq^{-1}) and ultra-large haze factor (98.5%), which can be potentially used as the front electrode in thin-film solar cells.

Acknowledgements

S.Q. Chen would like to thank the China Scholarship Council/Queen Mary University of London joint PhD scholarship program. Pilkington-NSG is specially thanked for providing glass substrates.

References

1. D. Ginley, H. Hosono, and D. C. Paine, *Handbook of Transparent Conductors*, Springer, New York, 2010.
2. B. Liu, X. Liang, J. Liang, L. Bai, H. Gao, Z. Chen, Y. Zhao, and X. Zhang, *Nanoscale*, 2015, **7**, 9816–24.
3. D. Wan, F. Huang, Y. Wang, X. Mou, and F. Xu, *ACS Appl. Mater. Interfaces*, 2010, **2**, 2147–2152.
4. S. Faÿ, J. Steinhauser, N. Oliveira, E. Vallat-Sauvain, and C. Ballif, *Thin Solid Films*, 2007, **515**, 8558–8561.
5. T. Shinagawa, K. Shibata, O. Shimomura, M. Chigane, R. Nomura, and M. Izaki, *J. Mater. Chem. C*, 2014, **2**, 2908.
6. J. Liu, X. Chen, J. Fang, Y. Zhao, and X. Zhang, *Sol. Energy Mater. Sol. Cells*, 2015, **138**, 41–50.
7. C. Battaglia, C.-M. Hsu, K. Söderström, J. Escarré, F.-J. Haug, M. Charrière, M. Boccard, M. Despeisse, D. T. L. Alexander, M. Cantoni, Y. Cui, and C. Ballif, *ACS Nano*, 2012, **6**, 2790–7.
8. http://www.products.cvdequipment.com/applications/boron_doped_zno_lpcvd_thin_film_coating/.
9. W. Chen, W. Cao, J. Hao, and K. Wang, *Mater. Lett.*, 2015, **139**, 98–100.
10. H. Sugimoto, H. Ohshima, and S. Inoue, *J. Polym. Sci. Part A Polym. Chem.*, 2003, **41**, 3549–3555.
11. P. Marchand, I. A. Hassan, I. P. Parkin, and C. J. Carmalt, *Dalt. Trans.*, 2013, **42**, 9406–9422.

12. S. Chen, G. Carraro, D. Barreca, A. Sapelkin, W. Chen, X. Huang, Q. Cheng, F. Zhang, and R. Binions, *J. Mater. Chem. A*, 2015, **3**, 13039–13049.
13. J. A. Manzi, C. E. Knapp, I. P. Parkin, and C. J. Carmalt, *Eur. J. Inorg. Chem.*, 2015, **2015**, 3658–3665.
14. S. D. Ponja, S. Sathasivam, I. P. Parkin, and C. J. Carmalt, *RSC Adv.*, 2014, **4**, 49723–49728.
15. S. Chen, N. Noor, I. P. Parkin, and R. Binions, *J. Mater. Chem. A*, 2014, **2**, 17174–17182.
16. C. S. McNally, D. P. Turner, A. N. Kulak, F. C. Meldrum, and G. Hyett, *Chem. Commun.*, 2012, **48**, 1490–1492.
17. S. Chen, R. M. Wilson, and R. Binions, *J. Mater. Chem. A*, 2015, **3**, 5794–5797.
18. G. Walters and I. P. Parkin, *Appl. Surf. Sci.*, 2009, **255**, 6555–6560.
19. X. J. Qin, L. Zhao, G. J. Shao, and N. Wang, *Thin Solid Films*, 2013, **542**, 144–149.
20. X.-G. Han, H.-Z. He, Q. Kuang, X. Zhou, X.-H. Zhang, T. Xu, Z.-X. Xie, and L.-S. Zheng, *J. Phys. Chem. C*, 2009, **113**, 584–589.
21. N. Qin, Q. Xiang, H. Zhao, J. Zhang, and J. Xu, *CrystEngComm*, 2014, **16**, 7062.
22. A. J. T. Naik, M. E. A. Warwick, S. J. A. Moniz, C. S. Blackman, I. P. Parkin, and R. Binions, *J. Mater. Chem. A*, 2013, **1**, 1827–1833.
23. http://www.engineeringtoolbox.com/liquids-densities-d_743.html.
24. M. Zhang, Y. Nakayama, and L. Pan, *Jpn. J. Appl. Phys.*, 2000, **39**, L1242–L1244.
25. M. R. Waugh, G. Hyett, and I. P. Parkin, *Chem. Vap. Depos.*, 2008, **14**, 366–372.
26. Y.-J. Choi and H.-H. Park, *J. Mater. Chem. C*, 2014, **2**, 98.
27. X. Zhou, Z.-X. Xie, Z.-Y. Jiang, Q. Kuang, S.-H. Zhang, T. Xu, R.-B. Huang, and L.-S. Zheng, *Chem. Commun.*, 2005, **1**, 5572–4.
28. Z. R. Tian, J. A. Voigt, J. Liu, B. McKenzie, M. J. McDermott, M. A. Rodriguez, H. Konishi, and H. Xu, *Nat. Mater.*, 2003, **2**, 821–6.
29. N. J. Nicholas, G. V Franks, and W. A. Ducker, *Langmuir*, 2012, **28**, 7189–96.
30. S. Das, K. Dutta, and A. Pramanik, *CrystEngComm*, 2013, **15**, 6349.
31. B. C. Jiao, X. D. Zhang, C. C. Wei, J. Sun, Q. Huang, and Y. Zhao, *Thin Solid Films*, 2011, **520**, 1323–1329.
32. L. Ding, M. Boccard, G. Bugnon, M. Benkhaira, S. Nicolay, M. Despeisse, F. Meillaud, and C. Ballif, *Sol. Energy Mater. Sol. Cells*, 2012, **98**, 331–336.
33. http://www.beneq.com/aerosol-equipment-general.html.
34. B. C. Cheng, Y. H. Xiao, G. S. Wu, and L. D. Zhang, *Adv. Funct. Mater.*, 2004, **14**, 913–919.
35. Q. Cheng and K. K. Ostrikov, *Chemphyschem*, 2012, **13**, 1535–41.
36. C.-L. Hsu, S.-J. Chang, Y.-R. Lin, S.-Y. Tsai, and I.-C. Chen, *Chem. Commun.*, 2005, 3571–3.
37. G. R. Li, T. Hu, G. L. Pan, T. Y. Yan, X. P. Gao, and H. Y. Zhu, *J. Phys. Chem. C*, 2008, **112**, 11859–11864.
38. K. Fink, *Phys. Chem. Chem. Phys.*, 2006, **8**, 1482–9.